Contributed Paper

Multi-Dimensional Structure of the Electric Field in Tokamak H-Mode

KASUYA Naohiro and ITOH Kimitaka

National Institute for Fusion Science, Toki, Gifu 509-5292, Japan

In tokamak H-mode, a large poloidal flow exists in an edge transport barrier, and the electrostatic potential and density profiles can be steep both in the radial and poloidal direction. Two-dimensional structures of the potential, density and flow velocity near the edge of a tokamak plasma are investigated. The model includes the nonlinearity in bulk-ion viscosity and turbulence-driven shear viscosity. For the case with a strong radial electric field (H-mode), a two-dimensional structure in a transport barrier is obtained, giving a poloidal shock with a solitary radial electric field profile. The poloidal electric field induces convective transport in the radial direction, and poloidal asymmetry makes the flux-surface-averaged particle flux direct inward with a pinch velocity on the order of 1 [m/s]. A large poloidal flow with radial shear enhances the inward pinch velocity. The abrupt increase of this inward ion and electron flux at the onset of L-to-H-mode transition explains the rapid establishment of the density pedestal at the transition.

Keywords:

poloidal shock structure, electric field, H-mode, inward particle pinch, shear viscosity

1. Introduction

Toroidal plasmas have nonlinear response and lead to complex phenomena [1]. The nonlinearity allows formation of a variety of structures. The structural transition to inhomogeneous profiles in toroidal plasmas has been the focus of numerous researches. A typical example of this is H-mode transition [2], key mechanisms of which include bifurcation of the electric field [3,4] and associated suppression of turbulence by electric field structures [5,6]. Thus significant attention has been devoted to studying the steep radial electric field structure in the L/H transition physics [7].

Although significant progress has been made in clarifying the radial electric field structure, several fundamental issues remain. For instance, the rapid establishment of the density profile pedestal after the onset of L/H transition [8] remains unexplained. The one-dimensional continuity equation is written as

$$\frac{\partial n}{\partial t} = -\nabla\left(nV - D_a\nabla n\right) + S, \tag{1}$$

where n, V, D_a and S are the density, flow velocity, diffusion coefficient and particle source, respectively [9]. The first and second term in the right hand side of Eq. (1) correspond to the convective and diffusive transport term, respectively. It is well known that turbulent diffusivity decreases rapidly after transition, so the coefficient D_a decreases, leading a large

gradient of n [10]. However, this reduced diffusion makes the time required to reach a steady state much longer than observed. One possible cause of the fast establishment of the pedestal is an increase of the inward particle pinch. In the steady state, peaked plasma profiles are often observed without a sufficient particle source, and this suggests the existence of an inward pinch having a velocity on the order of 1 [m/s] [9,11]. The origin of the inward pinch has yet to be unresolved. Ware pinch driven by the toroidal electric field [12] alone cannot account for the peaked density profile, because the inward pinch is observed even in helical systems [13,14] and noninductively current driven tokamaks [15]. In addition, the enhancement of the pinch velocity is observed after the L/H transition [16]. There have been several attempts to explain this "anomalous" inward pinch [17-26]. Turbulent transport produces the inward particle pinch in the core region of plasmas, but in the H-mode transport barrier, fluctuations are suppressed, so another mechanism must be introduced to explain the inward particle pinch.

Another issue is the formation of a poloidal shock associated with a large poloidal flow. In theoretical studies in which only the poloidal variation was taken and the radial structure was neglected, it was predicted that the poloidal shock can appear in H-mode plasmas [27,28]. The poloidal shock is a steady density or potential jump in the poloidal direction, resulting from plasma compressibility and toroidicity. Some

experiments have indicated the existence of poloidal asymmetry [29,30]. The poloidal electric field generates convective transport in the radial direction by the $E \times B$ drift. If such a poloidal shock exists, a large inward particle pinch could be induced [1], and may influence the pedestal formation. This consideration has motivated the study of two-dimensional structures at the transport barrier. Some progress has been reported [31,32], but our understanding of these structures is far from satisfactory.

In this paper, we study the two-dimensional structure of the electrostatic potential, density and flow velocity near the edge of a tokamak plasma. A set of equations, which describes the transition to the steep radial electric field structure as well as the poloidal inhomogeneity, is derived by considering the nonlinearity in bulk-ion viscosity and (turbulence-driven) shear viscosity. By introducing an ordering (shock ordering [27]), the coupled nonlinear partial differential equations are divided into two parts. The first is an ordinary differential equation that governs the steep radial structure of the radial electric field (or poloidal flow). The bifurcation and transition of the poloidally averaged part of the radial electric field are obtained from this equation. The second is a nonlinear partial differential equation that governs the poloidal asymmetry of the flow (including the poloidal shock). In the latter equation, the radial structure of the strong radial electric field is already given by the former equation. Thus the theoretical framework that describes the bifurcation of the radial structure as well as the poloidal inhomogeneity is obtained. A two-dimensional structure generates the inward particle pinch, and gives a possible explanation for the rapid establishment of the edge pedestal on L/H transition. It is emphasized that the validity of the L/H transition theory, which has been based on one-dimensional analyses, is confirmed by this two-dimensional analysis. The paper is organized as follows. Previous works on steep structures in the radial and poloidal direction are briefly introduced in Sec. **2**. Derivation of the model equations is described in Sec. **3**. In Sec. **4**, solutions of two-dimensional structures are described in the case with a weak and strong radial electric field. Enhancement of the inward particle pinch at the onset of L/H transition and experiments to identify the two-dimensional structure are discussed in Sec. **5**. The summary is presented in Sec. **6**.

2. A Brief Overview of One-Dimensional Analyses

First, we will revisit two examples of a steep structure in one direction. One is a radial solitary structure induced by electrode biasing, and the other is a poloidal shock structure.

2.1 Radial solitary structure

In H-mode, the density or temperature profile near the plasma edge becomes steeper and forms a pedestal. The radial electric field plays an important role in the improved confinement [7]. The steep gradient of the radial electric field is found to decrease the anomalous transport [5,6]. The radial electric field becomes large in the transport barrier, so the radial electric field and the toroidal magnetic field create a

large $E \times B$ flow velocity pointing in the poloidal direction. The poloidal Mach number $M_p = E_r / (v_{ti} B_p)$ increases to the order of unity in H-mode, where E_r is the radial electric field, $v_{ti} = \sqrt{2T_i/m_i}$ is the thermal velocity of ions, T_i is the ion temperature, m_i is the ion mass and B_p is the poloidal magnetic field. Most of the previous studies were concerned with clarifying the details of the structural formation mechanism in the radial direction.

Nonlinear mechanisms of the steep radial electric field structure have been studied by biased limiter experiments in which an externally driven H-mode transition was induced [33,34]. An externally imposed voltage changes the radial electric field structure in the same way as in spontaneous H-modes. Imposing a radial electric field by an electrode inserted into a plasma gives a transition to an improved confinement state when the voltage applied to the electrode is larger than the threshold value. This transition is characterized by a sudden change of the radial electric field structure from a flat one to a peaked one. Theoretical studies have clarified the formation mechanism of this solitary radial electric field structure [35,36]. The radial electric field structure is calculated from the charge conservation law,

$$\frac{\partial}{\partial t} E_r = - \frac{1}{\varepsilon_0 \varepsilon_\perp} \left(J_{visc} + J_r - J_{ext} \right), \qquad (2)$$

where J_{visc} is the current driven by shear viscosity, J_r is the local current, J_{ext} includes the current driven into the electrode by the external circuit and ion orbit loss current, etc., ε_0 is the vacuum susceptibility, and $\varepsilon_\perp$ is the dielectric constant of a magnetized plasma. The nonlinearity of the local current has a major effect on the radial electric field structural bifurcation. One solution of the radial electric field structure is shown in Fig.1. A stable solitary structure is obtained. This structure has a large gradient, and this characteristic is typical in H-mode.
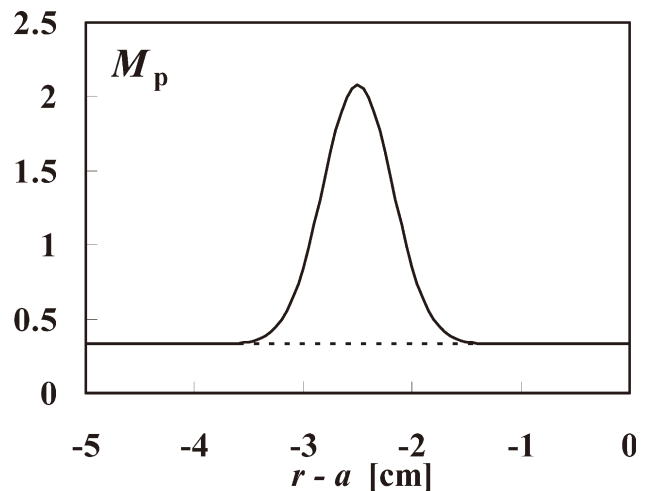

Fig. 1   Solitary radial structure of the radial electric field (translated into M_p) in electrode biasing H-mode. The positions $r - a = -5$ and 0 [cm] are where the electrode and the limiter are placed, respectively.

The nonlinearity in the relationship between the radial electric field and the radial current has been examined explicitly in other toroidal plasma experiments [37].

2.2 Poloidal shock structure

In a toroidal plasma, the poloidal structure can be asymmetric as well as the radial structure. In the tokamak edge region in H-mode, the poloidal flow increases to $M_p > 1$, and appearance of a poloidal shock structure in the potential and density profile has been predicted theoretically with such a large poloidal flow [27,28]. This shock structure is a steady jump structure. In ref. [27] the poloidal shock structure in a single magnetic flux surface is derived from the momentum balance equation,

$$m_i n \frac{d}{dt} \vec{V}_i = \vec{J} \times \vec{B} - \vec{\nabla}(p_i + p_e) - \vec{\nabla} \cdot \vec{\pi}_i, \qquad (3)$$

where $\vec{V}_i$ is the flow velocity, $\vec{J}$ is the plasma current, p_i and p_e are the ion and electron pressure and $\vec{\pi}_i$ is the viscosity tensor of ions. The flow is compressible with a supersonic poloidal flow, so the convective derivative term becomes effective in this situation. The parallel component of Eq. (3) can be written to be

$$\frac{2}{3} D \frac{\partial \chi}{\partial \theta} + \left(1 - M_p^2\right)\chi + 2A\left(\chi^2 - \langle \chi^2 \rangle\right)$$
$$= \varepsilon \left[2M_p^2 \cos\theta + D\sin\theta \right], \qquad (4)$$

using

$$\chi \equiv \ln\left(\frac{n}{\bar{n}}\right).$$

Details of the derivation of Eq. (4) and the definition of each constant will be described in section 3. In the left hand side of Eq. (4), the first term is derived from bulk viscosity arising from pressure anisotropy between the parallel and perpendicular direction, the second term represents the difference between the convective derivative $(V \cdot \nabla)V$ and pressure gradient ∇p, and the third term is nonlinearity coming from the higher order of χ. The terms in the right hand side of Eq. (4), which are derived from toroidicity in this system, are proportional to the inverse aspect ratio ε and have sinusoidal dependence.

Solving Eq. (4), shock solutions can be obtained. Figure 2 (a) shows shock profiles when $D = 0.1$. Large density jumps appear near the position $\theta = 0$ (the low field side of tokamak) when $M_p \sim 1$. Figure 2 (b) shows the profile of the poloidal electric field when $M_p = 1.0$. The large poloidal field is localized at the shock position. The shock structure is characterized by the steepness and the position of the shock. The position of the shock can be represented analytically as
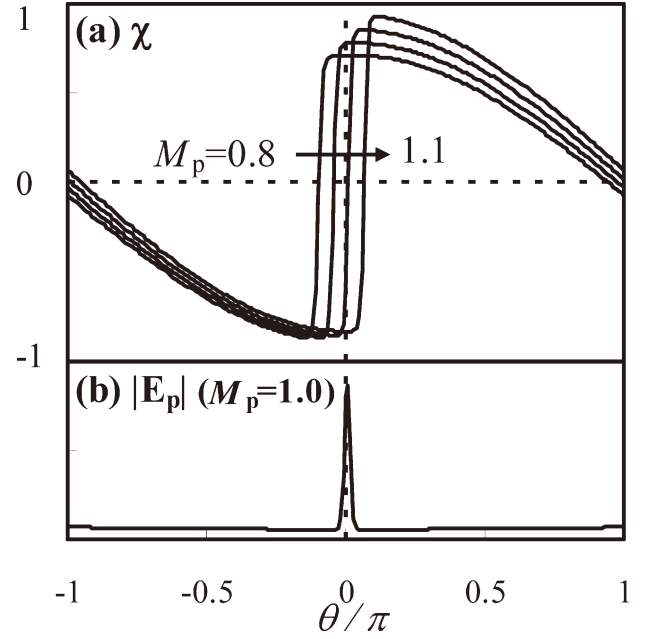

Fig. 2   (a) Profiles of the density perturbation χ when $D = 0.1$. The cases with $M_p = 0.8$, 0.9, 1.0 and 1.1 are plotted. (b) Profile of the poloidal electric field calculated from the perturbation profile (a) of the case $M_p = 1.0$.

$$\theta_{\text{shock}} = -\theta_\alpha + 2 \arcsin \frac{\pi \left| 1 - M_p^2 \right|}{8\sqrt{A\varepsilon \sqrt{2M_p^2 + D^2}}}, \qquad (5)$$

where

$$\tan\theta_\alpha = -\frac{D}{2M_p^2}.$$

The shock position depends on M_p, so as the poloidal flow increases, the shock position changes correspondingly. The maximum θ gradient is given at the shock position as

$$\left. \frac{\partial \chi}{\partial \theta} \right|_{\text{max}}$$
$$= \frac{3\varepsilon}{2D} \sqrt{2M_p^2 + D^2} \left[\cos\left(\theta_{\text{shock}} + \theta_\alpha\right) + 1 \right]. \qquad (6)$$

The steepness of the shock is inversely proportional to D when $D \ll 1$.

The shock formation mechanism can be explained as follows. There are two states for the poloidal structure. One is the ∇p-dominant state. When the poloidal flow is subsonic ($M_p \ll 1$), the convective derivative term is negligible, so the ∇p term determines the state. The ∇p smoothes the profile, so the poloidal structure becomes homogeneous. When the poloidal flow is supersonic ($M_p \gg 1$), the convective derivative term becomes dominant, and condition $(V \cdot \nabla)V = 0$ determines the profile. This state is another state, the $(V \cdot \nabla)V$-dominant state.

The velocity is conserved along the flow line, so the density is larger in the region where the magnetic field is stronger. When $M_p \sim 1$, the ∇p term and the $(V \cdot \nabla)V$ term are competitive, and nonlinearity of the higher order of χ appears. In this situation, the ∇p-dominant and $(V \cdot \nabla)V$-dominant states both exist, and shock appears at the boundary between these regions.

3. Model Equation
3.1 Geometry and momentum balance for the two-dimensional problem

To evaluate the two-dimensional structure in tokamak edge plasma, the flux-surface-averaged equations are inappropriate. We consider a large aspect ratio tokamak with a circular cross-section, and the coordinates (r, θ, ζ) are used (r: radius; θ: poloidal angle; ζ: toroidal angle). Poloidal variations of the density and the electrostatic potential are considered, but that of the temperature is neglected. Electrons are isothermal, ions are adiabatic, and $n_i = n_e \equiv n$ is assumed, where n_i and n_e are the ion and electron density, respectively. The derivation of the model equation follows Ref. [27], but the radial flow and shear viscosity are taken into account here [38]. By these terms, the radial and poloidal structures are coupled with each other. The structures are governed by the momentum balance equation

$$m_i n \frac{d}{dt} \vec{V}_i = \vec{J} \times \vec{B} - \vec{\nabla}\left(p_i + p_e\right) - \left(\vec{\nabla} \cdot \vec{\pi}_i\right)_{\text{bulk}} - \left(\vec{\nabla} \cdot \vec{\pi}_i\right)_{\text{shear}} . \quad (7)$$

The viscosity $\vec{\pi}_i$ is divided into two terms: the bulk viscosity given by a neoclassical process [39], and shear viscosity given by an anomalous process [1]. The viscosity of electrons is neglected because it is smaller by a factor on the order of $\sqrt{m_e/m_i}$. Pressure $p = nT$, and constant temperature T is assumed. The perpendicular flow is given by the $\boldsymbol{E} \times \boldsymbol{B}$ drift here, and the flow velocity is written as

$$\vec{V} = \vec{V}_{/\!/} + \frac{\vec{E} \times \vec{B}}{B^2} = \begin{pmatrix} -\dfrac{I}{rRB^2}\dfrac{\partial \Phi}{\partial \theta} \\[2mm] \dfrac{KB_p}{n} \\[2mm] \dfrac{KB_\zeta}{n} - \dfrac{1}{B_p}\dfrac{\partial \Phi}{\partial r} \end{pmatrix}, \quad (8)$$

where Φ is the electrostatic potential,

$$K = \frac{nV_p}{B_p},$$

corresponding to the poloidal flow, and

$$I = R^2\vec{B} \cdot \nabla\zeta ,$$

The toroidal symmetry is utilized in this description. The parallel component and averaged poloidal component of the

momentum balance Eq. (7) are given to be

$$-\frac{nI}{KB^2 rR}\frac{\partial \Phi}{\partial \theta}\frac{\partial}{\partial r}\left[\frac{1}{2}\left(\frac{KB}{n}\right)^2\right] + \frac{B_p}{r}\frac{\partial}{\partial \theta}\left[\frac{1}{2}\left(\frac{KB}{n}\right)^2\right]$$

$$+\frac{IB_\zeta}{B^2 rR}\frac{\partial \Phi}{\partial \theta}\frac{\partial}{\partial r}\left[\frac{I}{RB_p B_\zeta}\frac{\partial \Phi}{\partial r}\right]$$

$$-\frac{KB_p B_\zeta}{nr}\frac{\partial}{\partial \theta}\left[\frac{I}{RB_p B_\zeta}\frac{\partial \Phi}{\partial r}\right]$$

$$= -\frac{B_p}{m_i r}\frac{\partial}{\partial \theta}\left(\frac{\langle p_e\rangle}{\langle n\rangle}\ln n + \frac{5}{2}\frac{\langle p_i\rangle}{\langle n^{5/3}\rangle}n^{2/3}\right)$$

$$-\frac{1}{m_i n}\left(\vec{B} \cdot \vec{\nabla} \cdot \vec{\pi}_i\right)_{\text{bulk}} - \frac{1}{m_i n}\left(\vec{B} \cdot \vec{\nabla} \cdot \vec{\pi}_i\right)_{\text{shear}} , \quad (9)$$

$$\left\langle -\frac{nI}{KB^2 rR}\frac{\partial \Phi}{\partial \theta}\frac{\partial}{\partial r}\left[\frac{1}{2}\left(\frac{KB_p}{n}\right)^2\right]\right.$$

$$\left. +\frac{B_p}{r}\frac{\partial}{\partial \theta}\left[\frac{1}{2}\left(\frac{KB_p}{n}\right)^2\right]\right\rangle$$

$$= \frac{1}{m_i}\left\langle\frac{JB_p B_\zeta}{n}\right\rangle - \frac{1}{m_i}\left\langle\frac{\vec{B}_p \cdot \vec{\nabla} \cdot \vec{\pi}_i}{n}\right\rangle_{\text{bulk}}$$

$$-\frac{1}{m_i}\left\langle\frac{\vec{B}_p \cdot \vec{\nabla} \cdot \vec{\pi}_i}{n}\right\rangle_{\text{shear}} , \quad (10)$$

where $\langle\ \rangle$ denotes the flux surface average. The radial flow is taken into account, so the $\partial\Phi/\partial\theta$ terms are involved in the left side of Eqs. (9) and (10). Using the viscosity tensor $\vec{\pi}_i = (p_{/\!/} - p_\perp)(\hat{b}\hat{b} - \vec{t}_i/3)$, where $(p_{/\!/} - p_\perp)$ is the pressure anisotropy, $\hat{b}$ is the unit vector parallel to the magnetic field and $\vec{t}$ is the unit tensor, the bulk viscosity term can be written as

$$\left(\vec{B} \cdot \vec{\nabla} \cdot \vec{\pi}_i\right)_{\text{bulk}} = \frac{2}{3}\frac{B_p}{r}\frac{\partial}{\partial \theta}\left(p_{/\!/} - p_\perp\right)$$

$$-\left(p_{/\!/} - p_\perp\right)\frac{B_p}{B}\frac{1}{r}\frac{\partial B}{\partial \theta} . \quad (11)$$

The first term of Eq. (11) is dominant, so only this term is kept in Eq. (9) hereafter. In contrast, the surface average is taken in Eq. (10), in which the second term of Eq. (11) remains. The pressure anisotropy, deduced from the drift kinetic equation with mass flow velocity, is as follows [40]:

$$p_{//} - p_{\perp}$$
$$= -2\sqrt{\pi}\, I_{\text{ps}} K m_{\text{i}} v_{\text{ti}} B \left(\frac{\partial}{\partial\theta} \ln B - \frac{2}{3}\frac{\partial}{\partial\theta} \ln n \right). \qquad (12)$$

The integral I_{ps} is

$$I_{\text{ps}} = \frac{1}{\pi} \int_0^{\infty} \mathrm{d}x\, x^2 e^{-x} \int_{-1}^{1} \mathrm{d}\eta \left(\frac{1}{2} - \frac{3\eta^2}{2} \right)^2 \frac{y/\sqrt{x}}{U_{\text{t}}^2 + \left(y/\sqrt{x} \right)^2} , \qquad (13)$$

where

$$y = \frac{r v_{\text{T}} B}{v_{\text{ti}} B_{\text{p}}} ,$$

$$U_{\text{t}} = G_{\text{r}} \left[\eta + \left(-\frac{E_{\text{r}}}{B} + V_{//} \frac{B_{\text{p}}}{B} \right) \Big/ \left(\sqrt{x}\, \frac{v_{\text{ti}} B_{\text{p}}}{B} \right) \right] ,$$

v_{T} is the characteristic collision frequency defined in Ref. [41], and G_{r} is a geometric factor, taken to be $G_{\text{r}} = 1$ in this paper. The shear viscosity is given by the second perpendicular derivative of the flow velocity, and is here simply given to be

$$\left(\vec{B} \cdot \vec{\nabla} \cdot \vec{\pi}_{\text{i}} \right)_{\text{shear}} = -m_{\text{i}} n \mu \vec{B} \cdot \nabla_{\perp}^2 \vec{V} , \qquad (14)$$

where μ is a shear viscosity coefficient. The coefficient μ depends on the radial electric field and has spatial variation, but we take it to be constant in space for simplicity. This is because we are focusing on the structural formation mechanism from the nonlinearity of each term. The structural formation mechanism from turbulent induction will be treated elsewhere. The Boltzmann relation

$$n = \bar{n} \exp \frac{e\Delta\Phi}{T_{\text{i}}} \qquad (15)$$

is adopted here to determine variables, where $\bar{f}$ and Δf represent the spatial average and perturbed parts of quantity f, respectively. The variables that must be determined from Eqs. (9), (10) and (15) are K, Φ and n, which have radial and poloidal variations. A variable $\chi = \ln(n/\bar{n})$ is introduced to represent density variation. From the Boltzmann relation Eq. (15), χ is directly related to the potential perturbation.

3.2 Ordering and decoupling of equations

In this paper, we are mainly concerned with the case in which the poloidal Mach number $M_{\text{p}} \sim 1$, and the steep structure in the poloidal direction is formed in this case, so the shock ordering, which is

$$\chi = O\!\left(\varepsilon^{1/2} \right), \qquad (16)$$

is adopted, where ε is the inverse aspect ratio. ε is considered to be small because the calculation is carried out only near the edge in a large aspect ratio tokamak. A condition

$$V_{\text{r}} / V_{\text{p}} \ll 1 \qquad (17)$$

is satisfied, even if a strong poloidal shock exists. This condition is confirmed, *a posteriori*, by the derived structures. Condition $V_{\text{r}} / V_{\text{p}} \ll 1$ makes the model equation simpler. The continuous equation in a steady state

$$\text{div}\left(n\vec{V} \right) = 0 \qquad (18)$$

shows K is a flux surface variable. Expanding Eq. (9) with χ, and taking up to O(ε), the following model equation is obtained:

$$-\hat{\mu} r^2 \frac{B_0}{B_{\text{p}}} \frac{\partial^2}{\partial r^2} \left\{ M_{\text{p}} \left[\exp\left(-\chi \right) - 1 \right] \right\}$$
$$+ \frac{2}{3} D \exp(-\chi) \frac{\partial^2 \chi}{\partial\theta^2} + \left(1 - M_{\text{p}}^2 \right) \frac{\partial\chi}{\partial\theta} + 2A \frac{\partial\chi}{\partial\theta}^2$$
$$= \varepsilon \left(\left\{ D - \hat{\mu}\frac{B_0}{B_{\text{p}}} \left[2r^2 \frac{\partial^2 M_{\text{p}}}{\partial r^2} + 4r \frac{\partial}{\partial r} M_{\text{p}} - 2M_{\text{p}} \right] \right\} \right.$$
$$\left. \cos\theta - 2M_{\text{p}}^2 \sin\theta \right), \qquad (19)$$

where

$$M_{\text{p}} = \frac{K B_0}{\bar{n}\, v_{\text{ti}} C_{\text{r}}} ,$$

$$\hat{\mu} = \frac{\mu}{r v_{\text{ti}} C_{\text{r}}} ,$$

$$A = \frac{M_{\text{p}}^2}{2} + \frac{5}{36\, C_{\text{r}}^2} ,$$

$$C_{\text{r}}^2 = \frac{1}{2} \left(\frac{5}{3} + \frac{T_{\text{e}}}{T_{\text{i}}} \right) ,$$

and

$$D = \frac{4\sqrt{\pi}\, I_{\text{ps}} K B_0}{3\bar{n}\, v_{\text{ti}} C_{\text{r}}^2} ,$$

Note that coefficient D has nonlinear dependency on M_{p}. Equation (19) is the equation for a strong toroidal damping

case when

$$M_p = \frac{I}{v_{ti} B_0 B_p C_r R} \frac{\partial \Phi}{\partial r} . \qquad (20)$$

In this case, M_p is proportional to the radial electric field. This condition is taken to simplify the model equation.

Now Eqs. (10), (15) and (19) determine the structure. This set is solved as follows. A profile of M_p is obtained by solving Eq. (10) independently from Eq. (19). Equation (10) is the same as the equation used for obtaining a radial profile of the radial electric field in the previous H-mode transition model [3,4,36] (see section 2.1). M_p (including the radial profile) is put into Eq.(19), and the two-dimensional structure of χ is obtained. Then the radial velocity is deduced.

Using these model equations, analysis is carried out in the region near the plasma edge, $r = (a - d) \sim a$, where $r = a$ is the position of the last closed flux surface. We consider the case in which the strong radial electric field is self-organized in the middle region of this domain, and choose the boundary condition to be $\chi = 0$ at $r = (a - d)$ and a. This is an idealization, considering that no perturbation exists outside of this region (such as in the edge barrier or biased region). Equation (19) is solved using previously obtained M_p profile [36]. (The calculations are performed using the following parameters: $R = 1.75$ [m], a = 0.46 [m], $B_0 = 2.35$ [T], $T_i = 40$ [eV], $I_p = 200$ [kA] and the boundaries $r - a = 0, -5$ [cm].)

Equation (19) includes characteristic structures both in the radial and poloidal direction. These structures are coupled with the shear viscosity. Properties of the characteristic structures explained as a one-dimensional structure problem in section 2.2 are derived from setting $\mu = 0$. There is no coupling in the radial direction, and the structures are closed in one flux surface. Equation (4) is given by integration of Eq. (19) with θ.

4. Two-Dimensional Structure

Equation (19) includes a shear viscosity term that couples the radial and poloidal structures so that two-dimensional structures can be obtained. The homogeneous (spatially constant M_p) case and the inhomogeneous case, corresponding to the L- and H-mode, respectively, are shown in this section. The solitary profile shown in Fig. 1 is used for the H-mode case, because this is a typical structure in H-mode, having an electric field with a large magnitude and large gradient.

4.1 Case of homogeneous M_p

We first study the case in which E_r is homogeneous to clarify the competition between the steepening by the $(V \cdot \nabla)V$-nonlinearity and the radial diffusion. In the absence of shear viscosity, the poloidal shock is predicted to appear as described in [27]. In L-mode the radial electric field is weak and the profile is rather flat. Figure 3 shows a profile of the potential perturbation when $M_p = 0.33$ and $\mu = 1.0$ [m²/s]. The potential perturbation is set to zero at the boundary $r - a = 0, -5$ [cm]. This profile shows that there is gentle variation both in the radial and poloidal direction. The case $M_p = 0.33$
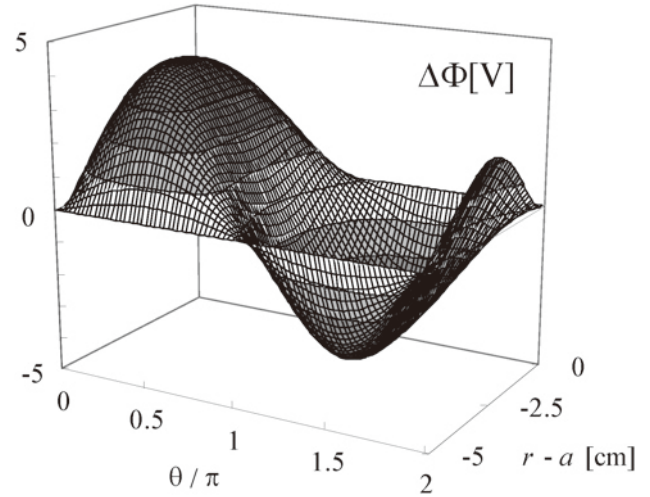

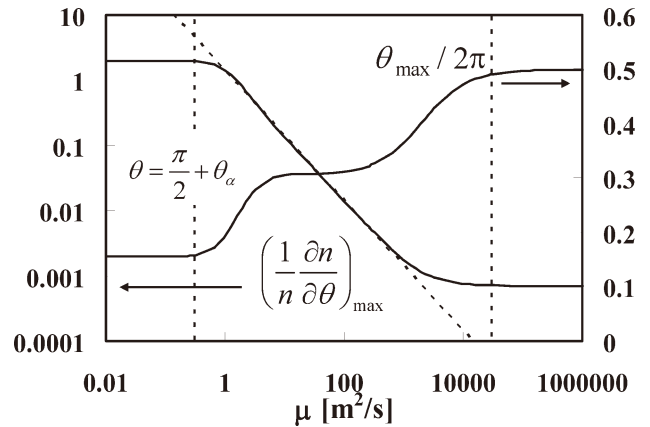Fig. 3   A two-dimensional potential perturbation profile with small and homogeneous E_r.

Fig. 4   Relationship between shear viscosity μ and the poloidal shock structure. The steepness and the position of the shock are important for describing the structure.

is used as the state just before the L/H transition. The value $M_p = 0.33$ means that a weak but constant radial electric field exists, so the potential difference between the boundaries is about 130 [V]. The ratio $\Delta\Phi/\Phi$ is about 6% at the maximum of the potential perturbation.

Shear viscosity μ controls the strength of coupling. Figure 4 shows the dependence of the maximum gradient of χ and the peak position on shear viscosity μ when $M_p = 1.2$, which is the case when the poloidal flow is large in the whole region near the plasma edge. In the shock regime,

$$\hat{\mu} < \mu_{ib} = \frac{D d^2 B_p}{12 a^2 M_p B_0} , \qquad (21)$$

radial coupling is weak, and the strong shock is formed in every flux surface except near the boundaries. The maximum gradient of χ and the peak position are those represented in Sec. 2.2. When the shear viscosity exceeds a threshold value

$\hat{\mu} > \mu_{ib}$, Eq. (19) can be simplified to

$$- \hat{\mu} r^2 \frac{B_0}{B_p} M_p \frac{\partial^2}{\partial r^2} (-\chi)$$

$$= \varepsilon \left[\left(D + 2\hat{\mu} \frac{B_0}{B_p} M_p \right) \cos\theta - 2 M_p^2 \sin\theta \right], \quad (22)$$

and its solution is

$$\chi(r, \theta) = \frac{\varepsilon \sqrt{D^2 + 4 M_p^4}}{2 \hat{\mu} a^2 M_p}$$

$$\frac{B_p}{B_0} (r - a)(r - a + d) \sin(\theta + \theta_\alpha) \quad (23)$$

for the intermediate regime. χ is inversely proportional to μ in this regime. Equation (23) gives the maximum value of χ at the point $\theta = \pi/2 + \theta_\alpha$, and thus the maximum gradient of χ is

$$\left(\frac{\partial \chi}{\partial \theta} \right)_{max} \sim \frac{\varepsilon v_{ti} C_r \sqrt{D^2 + 4 M_p^4}}{8 a M_p} \frac{B_p}{B_0} d^2 \frac{1}{\mu} \quad (24)$$

at the point $\theta = \pi - \theta_\alpha$. When the shear viscosity is very strong, i.e.,

$$\hat{\mu} B_0 / B_p \gg 1, \quad (25)$$

Eq. (22) gives

$$\chi(r, \theta) \sim \frac{\varepsilon}{a^2} (r - a)(r - a + d) \cos\theta, \quad (26)$$

which has no dependence on μ and M_p. No strong shock appears in this case. The maximum of χ is given at the point $\theta = \pi$, and the maximum gradient of χ becomes

$$\left(\frac{\partial \chi}{\partial \theta} \right)_{max} \sim \frac{\varepsilon d^2}{4 a^2} \quad (27)$$

at the point $\theta = \pi/2$.

In this way, the magnitude of μ determines the two-dimensional structure. Experimentally μ is estimated to be around 10^0 [m²/s] from transport analysis on CHS [42] or from the peak structure of the radial electric field in electrode biasing H-mode on TEXTOR [43]. Therefore, the plasmas in experimental devices are expected to be in the intermediate region. We takes $\mu = 1.0$ [m²/s] in the following calculations.

4.2 Cases of inhomogeneous M_p

We next study the two-dimensional structure by employing the solitary structures of the radial electric field, which
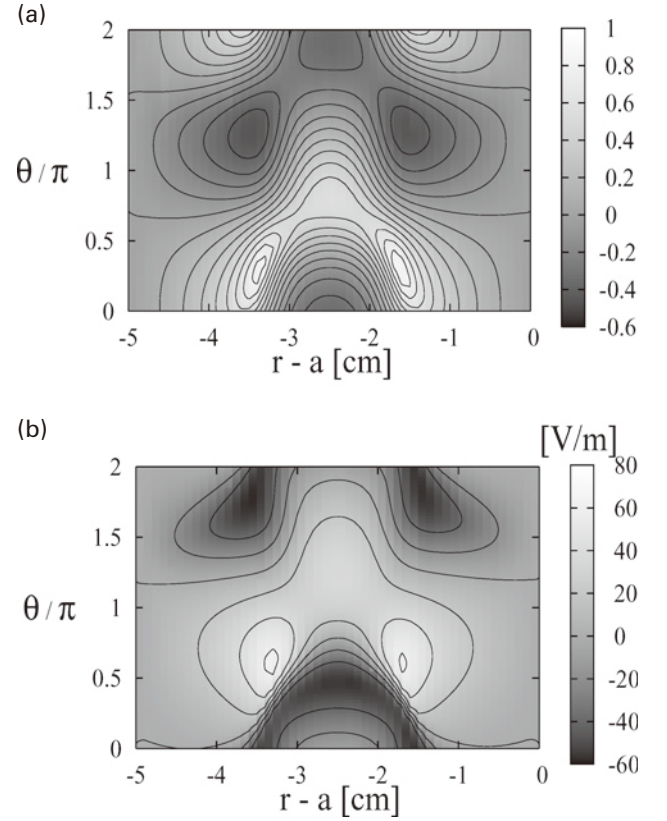

Fig. 5 A two-dimensional structure of the logarithm of density perturbation (a) and poloidal electric field (b) with strong and inhomogeneous E_r.

appear in the biased electrode experiments or in the H-mode edge barriers. Profiles of M_p are shown in Fig. 1, which is taken to illustrate the bifurcation of the radial electric field [36]. Under this condition, Eq. (19) is solved. Figure 5 (a) shows an χ profile, which is the logarithm of the density perturbation. The parameters are the same as in Fig. 3. Figure 5 (b) shows a profile of the poloidal electric field calculated from Fig. 5 (a) using the Boltzmann relation in Eq. (15). The region where M_p has a large value is localized in the middle of the shear region, so a localized large poloidal electric field exists at the points of the shock that have large M_p. In addition, the magnitude of M_p varies in the radial direction, and the poloidal position of the shock varies in the radial direction accordingly. We conclude that the two-dimensional structure of the edge transport barrier exists and influences the plasma flow, for the plasma parameters that are relevant to the H-mode confinement.

Comparison between the strong inhomogeneous E_r case and the weak homogeneous E_r case clarifies the formation of the localized steep two-dimensional structure. The strong E_r case has an E_r profile with a peak in the middle of the calculated region, although the weak E_r case has a spatially constant profile. The strong E_r case has a large potential perturbation (the maximum value $\Delta\Phi_{max} = 50$ [V] in this case), and a large localized poloidal electric field in which the poloidal flow shear is strong (the maximum value $E_{pmax} = 63$

[V/m]). This large poloidal electric field generates a large $E \times B$ flow pointing in the radial direction (the maximum value $V_{rmax} = 28$ [m/s]). In the weak E_r case, the values are $\Delta\Phi_{max} = 4$ [V], $E_{pmax} = 9$ [V/m] and $V_{rmax} = 4$ [m/s], respectively, which are one order smaller than in the strong E_r case.

5. Discussion

In this section, we discuss the impact of this two-dimensional structure on the formation of the pedestal of the transport barrier. The poloidal structure is found to generate radial flow much larger than 1 [m/s], but this large flow region is poloidally localized and the flow changes its direction according to the poloidal position. We calculate the flux-surface-averaged flux in the radial direction as

$$\left\langle nV_r \right\rangle = \left\langle n\frac{E_p}{B} \right\rangle$$

$$= \frac{\bar{n}}{2\pi r}\frac{T_i}{eB_0}\int \frac{\partial}{\partial\theta}\left[\exp\left(\frac{e\Delta\Phi}{T_i}\right)\right](1+\varepsilon\cos\theta)^2\,d\theta$$

(28)

by using the two-dimensional solution. Figure 6 represents the radial profiles of the flux-surface-averaged radial flux in the strong and weak E_r case, respectively. The radial flux has a negative value, so it points inward to the plasma center. The inward flux arises from poloidal asymmetry, so an inward pinch velocity $V_r \sim 1$ [m/s] exists even in the case with weak E_r. In the case with strong E_r, not only the large magnitude of poloidal flow but also the gradient and curvature of poloidal flow increase the inward pinch velocity. Figure 6 shows that the radial flux has a maximum in the radial position where the poloidal flow shear is larger. That is coming from the form of the shear viscosity in Eq. (14) that combines the poloidal asymmetry of magnetic field B and the gradient and curvature of the flow velocity.

The analysis of the two-dimensional structure reveals the existence of an inward particle pinch flow arising from poloidal asymmetry in the tokamak. This finding has a large impact on transport. Figure 7 (a) shows the relationship between the maximum of M_p and the particle pinch velocity. A moderate inward pinch velocity $V_r \sim 1$ [m/s] exists even in the weak E_r case (like the L-mode). This velocity is equivalent to that observed in experiments. In the strong E_r case, which is relevant to the H-mode or biased electrode experiments, a larger radial flow (inward pinch) is induced. The M_p profiles given to calculate Fig. 7 (a) is what is shown in Fig. 7 (b), and the increases in the maximum of M_p from 0.3 to 2.0 correspond to the transition of the E_r structure from flat to the peaked (solitary). The increase of the maximum of M_p leads to an increase of the inward convective particle flux.

The increase of the inward convective particle flux has a large impact on the pedestal formation on the L/H transition. In the L/H transition, M_p changes abruptly, so that the
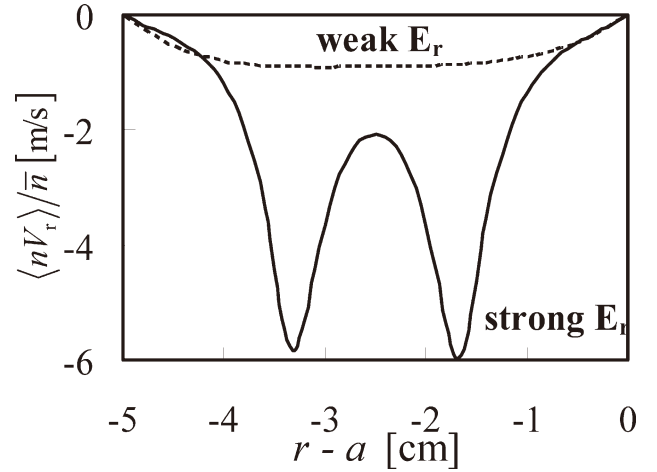

Fig. 6   Radial profiles of the flux-surface-averaged particle flux in the case of weak homogeneous and strong inhomogeneous E_r.
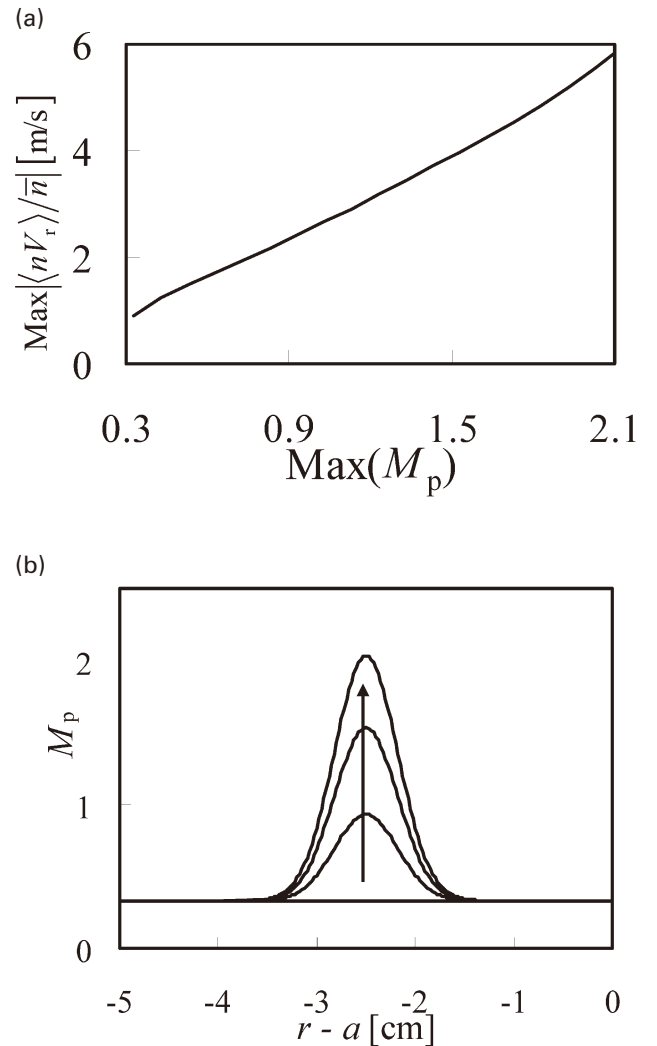

Fig. 7   (a) Relationship between the maximum of M_p and the particle pinch velocity. Increases of the maximum of M_p correspond to increases of the peak height of M_p as shown in (b).

convective transport changes abruptly in the transport barrier region at the same time. The suppression of transport and reduction of diffusive transport occur in the transport barrier. The reduction of the diffusion coefficient explains steepening of the H-mode pedestal, but the time constant of the pedestal formation is difficult to explain. That is, the necessary time for reaching the final pedestal gradient in the region with the width δ is given by $\tau = \delta^2/D_a$, where D_a is the reduced transport coefficient in the H-mode. It takes a longer time to form the pedestal ($\tau = 25$ [ms] when $\delta = 5$ [cm] and $D_a = 0.1$ [m^2/s]). The H-mode pedestal can be formed in a much shorter time $\tau \ll 10$ [ms] [8]. If the convective velocity increases abruptly, the time constant of the pedestal formation is $\tau = \delta/V$ ($\tau = 5$ [ms] when $\delta = 5$ [cm] and $V = 10$ [m/s]), so a sudden increase of the inward pinch flux is candidate for the cause of the rapid H-mode pedestal formation.

Finally, we will discuss how to confirm the two-dimensional structure in experiments. There are few measurements of the poloidal structure. In the CCT tokamak, the poloidal density profile was measured in electrode biasing H-mode [29]. The result showed poloidal variations that changed corresponding to the direction of the poloidal flow. However, it is not clear whether these variations arose from poloidal asymmetry or deviations in the measurements. If the measurements were carried out on different flux surfaces, it is expected to show some kind of inhomogeneity. Therefore, to observe the poloidal structure, it is necessary to identify measurement points on the same flux surface. This is not easy in every experimental device. Up-down asymmetry is the most important characteristic of the two-dimensional structure obtained in this paper, so confirmation of this asymmetry is needed. One alternative way to accomplish this is to scan the density or potential profiles on the different major radius R locations. Measurements in different locations reveal different up-down asymmetries, provide that a two-dimensional structure exists. This is because the shock position is localized at one poloidal position. In addition, the shock position differs in accordance with M_p, so controlling the flow velocity by electrode biasing will be illuminating to confirm the structure. Adjusting the applied voltage between the electrode and the limiter can make it possible to observe the shock on a cord of measurement, which cannot be moved freely in usual.

6. Summary

In summary, multidimensionality was introduced into the H-mode barrier physics in tokamaks. The radial steep structure in H-mode and the poloidal shock structure with the large poloidal flow were taken into account in a self-sustained system. The model equations with shear viscosity were derived. The magnitude of the shear viscosity determines the steepness and the position of the shock structure. In shock ordering, the structure of the flux-surface-averaged part is solved first, and using this M_p profile, a two-dimensional structure can be obtained iteratively. The one-dimensional model that has been used to study the L/H transition condition [7] is validated by this two-dimensional analysis. The radial solitary structure of the strong radial electric field was found to be associated with the poloidal shock structure for the parameters that are relevant to H-mode plasmas. The ion and electron inward pinch flux exists, and has a magnitude of O(10^0) [m/s] in the H-mode transport barrier. Abrupt increase of this convective transport at the onset of transition was predicted by this theory, which provides a new explanation of rapid H-mode pedestal formation.

We applied some simplifications to calculate the two-dimensional structure. The equation for a strong toroidal damping case is solved here. In this case M_p is proportional to the radial electric field. There is no qualitative difference compared with the general flow case [27], but in general, the parallel and poloidal flow are coupled with each other, so the determination of the flow must be treated more explicitly in Eq. (9). The different mobility between ions and electrons is included in Eq. (9), but deviation from the Boltzmann relation of ions is not considered. Our main interest is the shock formation, so these simplifications are made. More quantitative analysis will be carried out in a future work.

References

[1] K. Itoh, S.-I. Itoh and A. Fukuyama, *Transport and Structural Formation in Plasmas* (IOP, Bristol, 1999).

[2] F. Wagner *et al.*, Phys. Rev. Lett. **49**, 1408 (1982).

[3] S.-I. Itoh and K. Itoh, Phys. Rev. Lett. **60**, 2276 (1988); S.-I. Itoh and K. Itoh, Nucl. Fusion **29**, 1031 (1989).

[4] K.C. Shaing and E.C. Crume, Phys. Rev. Lett. **63**, 2369 (1989).

[5] S.-I. Itoh and K. Itoh, J. Phys. Soc. Jpn. **59**, 3815 (1990).

[6] H. Biglari, P.H. Diamond and P.W. Terry, Phys. Fluids B **2**, 1 (1990).

[7] See reviews, e.g. K. Itoh and S.-I. Itoh, Plasma Phys. Control. Fusion **38**, 1 (1996); K.H. Burrel, Phys. Plasmas **4**, 1499 (1997).

[8] F. Wagner *et al.*, in *Proceeedings of the 13th International Conference on Plasma Physics and Controlled Nucler Fusion Research, Washington, 1990* (IAEA, Vienna, 1991) Vol. 1, p. 277.

[9] B. Coppi and N. Sharky, Nucl. Fusion **21**, 1363 (1981).

[10] P. Gohil, Plasma Phys. Control. Fusion **44**, A37 (2002).

[11] F. Wagner and U. Stroth, Plasma Phys. Control. Fusion **35**, 1321 (1993).

[12] A.A. Ware, Phys. Rev. Lett. **25**, 916 (1970).

[13] U. Stroth *et al.*, Phys. Rev. Lett. **82**, 928 (1999).

[14] H. Iguchi *et al.*, Plasma Phys. Control. Fusion **36**, 1091

(1994).

[15] G.T. Hoang *et al.*, Phys. Rev. Lett. **90**, 155002 (2003).

[16] J.E. Rice *et al.*, Phys. Plasmas **4**, 1605 (1997).

[17] S.-I. Itoh, J. Phys. Soc. Japan **59**, 3431 (1990).

[18] R.K. Varma, Plasma Phys. Control. Fusion **40**, 1999 (1998).

[19] S. Puri, Plasma Phys. Control. Fusion **41**, L35 (1999).

[20] K.C. Shaing and R.D. Hazeltine, Phys. Fluids B **2**, 2353 (1990).

[21] B. Coppi and C. Spight, Phys. Rev. Lett. **41**, 551 (1978).

[22] R.R. Dominguez, Phys. Fluids B **5**, 1782 (1993).

[23] F. Jenko, Phys. Plasmas **7**, 514 (2000).

[24] J. Nycander and V.V. Yankov, Phys. Plasmas **2**, 2874 (1995).

[25] M.B. Isichenko, A.V. Gruzinov, P.H. Diamond and P.N. Yushmanov, Phys. Plasmas **3**, 1916 (1996).

[26] X. Garbet *et al.*, Phys. Rev. Lett. **91**, 035001 (2003).

[27] K.C. Shaing, R.D. Hazeltine and H. Sanuki, Phys. Fluids B **4**, 404 (1992).

[28] T. Taniuti *et al.*, J. Phys. Soc. Jpn. **61**, 568 (1992).

[29] R.J. Taylor, P. Pribyl, G.R. Tynan and B.C. Wells, in *Proceedings of 15th International Conference on Plasma Physics and Controlled Nuclear Fusion Research, Seville, 1994* (IAEA, Vienna, 1995) Vol. 2, p. 127.

[30] G.R. Tynan *et al.*, Plasma Phys. Control. Fusion **38**, 1301 (1996).

[31] M.J. Schaffer *et al.*, Phys. Plasmas **8**, 2118 (2001).

[32] W.M. Stacey, Phys. Plasmas **9**, 3874 (2002).

[33] R.J. Taylor *et al.*, Phys. Rev. Lett. **63**, 2365 (1989).

[34] R.R. Weynants *et al.*, Nucl. Fusion **32**, 837 (1992).

[35] K. Itoh, S.-I. Itoh, M. Yagi and A. Fukuyama, Phys. Plasmas **5**, 4121 (1998).

[36] N. Kasuya, K. Itoh and Y. Takase, Nucl. Fusion **43**, 244 (2003).

[37] A. Fujisawa *et al.*, Phys. Rev. Lett. **79**, 1054 (1997).

[38] N. Kasuya, K. Itoh and Y. Takase, J. Plasma Fusion Res. SERIES **6**, 283 (2004).

[39] K.C. Shaing, E.C. Crume and W.A. Houlberg, Phys. Fluids B **2**, 1492 (1990).

[40] K.C. Shaing, Phys. Fluids B **2**, 2847 (1990).

[41] S.P. Hirshman and D.J. Sigmar, Nucl. Fusion **21**, 1079 (1981).

[42] K. Ida and N. Nakajima, Phys. Plasmas **4**, 310 (1997).

[43] N. Kasuya, Ph. D. Thesis, Univ. Tokyo, 2003.